ELSEVIER

Mesoscale eddies in the northern South China Sea

Chau-Ron Wu*, Tzu-Ling Chiang

Department of Earth Sciences, National Taiwan Normal University, 88, Section 4 Ting-Chou Road, Taipei 116, Taiwan, ROC

Abstract

A fine-grid resolution model with realistic bathymetry and forcing has been developed to study the characteristics of the mesoscale eddies for the northern South China Sea (SCS). The SCS model derives its open-boundary conditions from a larger-scale model, which minimizes errors related to the uncertainty of the Kuroshio intrusion at the open boundaries. The model results are consistent with previous observations. Model sea-surface height anomaly demonstrates that the hydrography and circulation in the northern SCS are modulated by westward-propagating mesoscale eddies originating in the vicinity of the Luzon Strait. This explains the observed intra-seasonal fluctuations at the SouthEast Asian Time-series Study (SEATS) station. The mesoscale eddies have the same propagation speed as baroclinic Rossby waves ($\sim$0.1 m s^{-1}). The periods of eddy shedding estimated from Strouhal number are around 40–50 days in December and 80–120 days in August, respectively. The seasonal variability of the Kuroshio intrusion results in more eddies in winter than in summer.
© 2007 Elsevier Ltd. All rights reserved.

Keywords: SEATS; South China Sea circulation; Mesoscale eddy; Luzon Strait; Eddy shedding; Seasonal variability of the Kuroshio intrusion

1. Introduction

The SouthEast Asian Time-series Study (SEATS) station is located at 18.25°N and 115.67°E (Fig. 1) in the northeastern South China Sea (SCS), where the local circulation is complicated because of the complex topography. The near-surface circulation is largely influenced by the seasonal reversal of the monsoonal winds, northeasterly in winter and southwesterly in summer. The SCS circulation also has an inter-annual variation related to El Niño/Southern Oscillation (ENSO) (e.g., Wu and Chang, 2005).

*Corresponding author. Tel.: +886 2 2934 7120x16; fax: +886 2 2933 3315.

E-mail address: cwu@ntnu.edu.tw (C.-R. Wu).

The SEATS region is the confluence of currents in the northern SCS, the Taiwan Strait, and the Kuroshio intrusion. The temperature of the surface layer at SEATS station responds to seasonal heating and cooling, thus showing annual variations. On the other hand, intra-seasonal fluctuations (40–120 days) prevail at the subsurface thermocline layer. Metzger and Hurlburt (2001) suggested that the intra-seasonal fluctuations are a manifestation of mesoscale eddies. These eddies originate in the vicinity of the Luzon Strait, propagate westward and modulate intermittently the circulation pattern in the area.

The North Equatorial Current bifurcates at about 13°N east of Philippines to form the northward-flowing Kuroshio and the southward-flowing Mindanao Current (Nitani, 1972; Qu and Lukas, 2003).

Fig. 1. The integrated domain of the South China Sea model with realistic bathymetry. The locations of the mooring station (asterisk), the SEATS station (triangle), and the SCS2 station (open circle) are also labeled in the plot.

Before reaching Taiwan, the Kuroshio occasionally makes a loop within the Luzon Strait, a deep gap in the western boundary (Nitani, 1972; Shaw, 1991; Qu, 2000). Shaw (1991) used hydrographic data to show that from October to January the Philippine Sea Water extended west as far as 115°E, up to 250 m, and along the continental margin south of China. Using sea-surface temperature (SST) maps from Advanced Very High Resolution Radiometer (AVHRR) data, Farris and Wimbush (1996) observed that Kuroshio intrudes most frequently during the October–January when the Philippine Sea Water is also found below the surface. Centurioni et al. (2004) used drifters to demonstrate that the surface water from the Philippine Sea intrudes into the SCS through the Luzon Strait between October and January when the winds are dominated by the northeast monsoon. Qu (2000) suggested that the Kuroshio intrusion is a year-round phenomenon. Recent moored current-meter and ship-board Acoustic Doppler Current Profilers (ADCP) data confirm that the westward branch of the Kuroshio intrudes into the Luzon Strait year round (Liang et al., 2003).

The intrusion does not take place within the entire Luzon Strait. The largest intrusion occurs at the southern portion of the strait. The Kuroshio intrudes into the SCS through the deepest channels of the Luzon Strait: the Balintany Channel and south of Babuyan Island (Liang et al., 2003; Centurioni et al., 2004). In addition, the intrusion occasionally appears to be associated with meso-scale eddies. Observational evidence for this meso-scale variability has recently become available (Li et al., 1998). The mesoscale eddies propagate westward and intermittently modulate the regional hydrography and circulation. The SEATS station records this mesoscale variability.

In this work, we present and discuss the characteristics of mesoscale eddies that originate in the vicinity of the Luzon Strait based on a fine-grid resolution SCS model with realistic topography and forcing.

2. The numerical model

The SCS model used here is the sigma-coordinate Princeton Ocean Model (POM; Blumberg and

Mellor, 1987). The three-dimensional, free-surface model solves the primitive equations for momentum, salt, and heat. It includes a 2.5-level turbulence closure by Mellor and Yamada (1982), and the horizontal mixing by Smagorinsky (1963). Fig. 1 shows the SCS model domain with realistic bathymetry. The horizontal grid size is $1/16°$, and there are 26 sigma levels in the vertical. At the open boundaries, the SCS model derives its boundary condition from a larger-scale East Asian Marginal Seas (EAMS; Wu and Hsin, 2005) model. The EAMS model is also based on the POM, and has a horizontal resolution of $1/8°$ and 26 sigma levels. The EAMS model domain extends from $99°E$ to $140°E$ in longitude, and from $0°N$ to $42°N$ in latitude. A detailed description of the EAMS model is given by Wu and Hsin (2005). The EAMS model has been validated with observed temperature and salinity data in the SCS, and with observed velocity data from ADCPs in the Taiwan Strait (Wu and Hsin, 2005).

The POM uses the mode-splitting technique, in which the vertically integrated governing equations (barotropic, external mode) are separated from the equations governing vertical structure (baroclinic, internal mode). The one-way coupling between the SCS and EAMS models is described below. The vertically averaged barotropic velocities on the open boundaries of the EAMS model are estimated by the Flather (1976) formulation:

$$\bar{u}_n = \bar{u}_n^0 + \sqrt{\frac{g}{H}}(\eta - \eta^0), \tag{1}$$

where $\bar{u}_n$ is the vertically averaged outward normal component of the velocity on the open boundary of the SCS model at time t, $\bar{u}_n^0$ is the vertically averaged normal component of the velocity on the open boundary at time t, estimated from the EAMS model. The model sea-surface height η is calculated from the continuity equation, and is located half of a grid inside the open boundary of the SCS model domain. The EAMS model sea-surface height η^0 is located on the open boundary of the SCS model. The water depth of the open boundary is H, and g is the gravitational acceleration. Baroclinic velocities on the open boundaries of the SCS model are determined using an inflow condition; daily baroclinic velocities from the EAMS model are spatially interpolated and assigned to the open lateral boundary grids of the SCS model. Temperature and salinity on the open boundaries are subject to upstream advection and, in case of inflow daily

EAMS profiles of temperature and salinity supply the upstream values.

The SCS model was initialized by the temperature and salinity fields of the EAMS model outputs of January 1999, and thereafter was subject to climatological forcing for 1 year. After the spin-up period, the SCS model was forced with QSCAT/NCEP (NASA Quick Scatterometer/NCEP) wind data sets. The blended QSCAT/NCEP wind stress data set constitute one of the most up-to-date sets high-resolution data sets of ocean surface winds. We adopted six hourly fields of zonal and meridional wind components, 10 m above sea level and with a resolution of $0.5° \times 0.5°$. These fields are derived from a space and time blend of QSCAT-DIRTH satellite scatterometer observations and NCEP analyses (Milliff et al., 1999). The SCS model was subject to wind stress at the sea surface and forcing at the open-ocean boundary (as described above) provided by the EAMS model, which also was driven by the QSCAT/NCEP wind forcing. The simulation period is from 1999 to 2003.

3. Results and discussions

3.1. Comparison between observation and simulation

A shallow mooring (T1) deployed in continental margin at $20.86°N$ and $113.70°E$ (see Fig. 1) from November 5, 2001 to March 21, 2002 is used to check the model velocity. Fig. 2A, from Yang (2006), shows time series of the observed 48-h low-pass eastward (U) and northward (V) velocity components at the T1 station. In general, the flow is barotropic up to 70 m, slightly decreasing in velocity with depth. Both U and V show significant intra-seasonal variations. U was westward in early November 2001, but alternated between east and west in late November 2001. The flow strengthened and became westward in December 2001, but suddenly reversed towards the east in late December 2001. The westward flow reappeared after the middle of January 2002, alternated between east and west during February 2002, and returned to westward thereafter. The V component shows a similar pattern with the U component, alternating north- and south-ward.

Fig. 2B shows the model-derived time series of the U and V velocity components at the same location of the T1 station. The magnitudes of the model velocity are comparable to observations. Model and observed velocities also are often in phase. Model
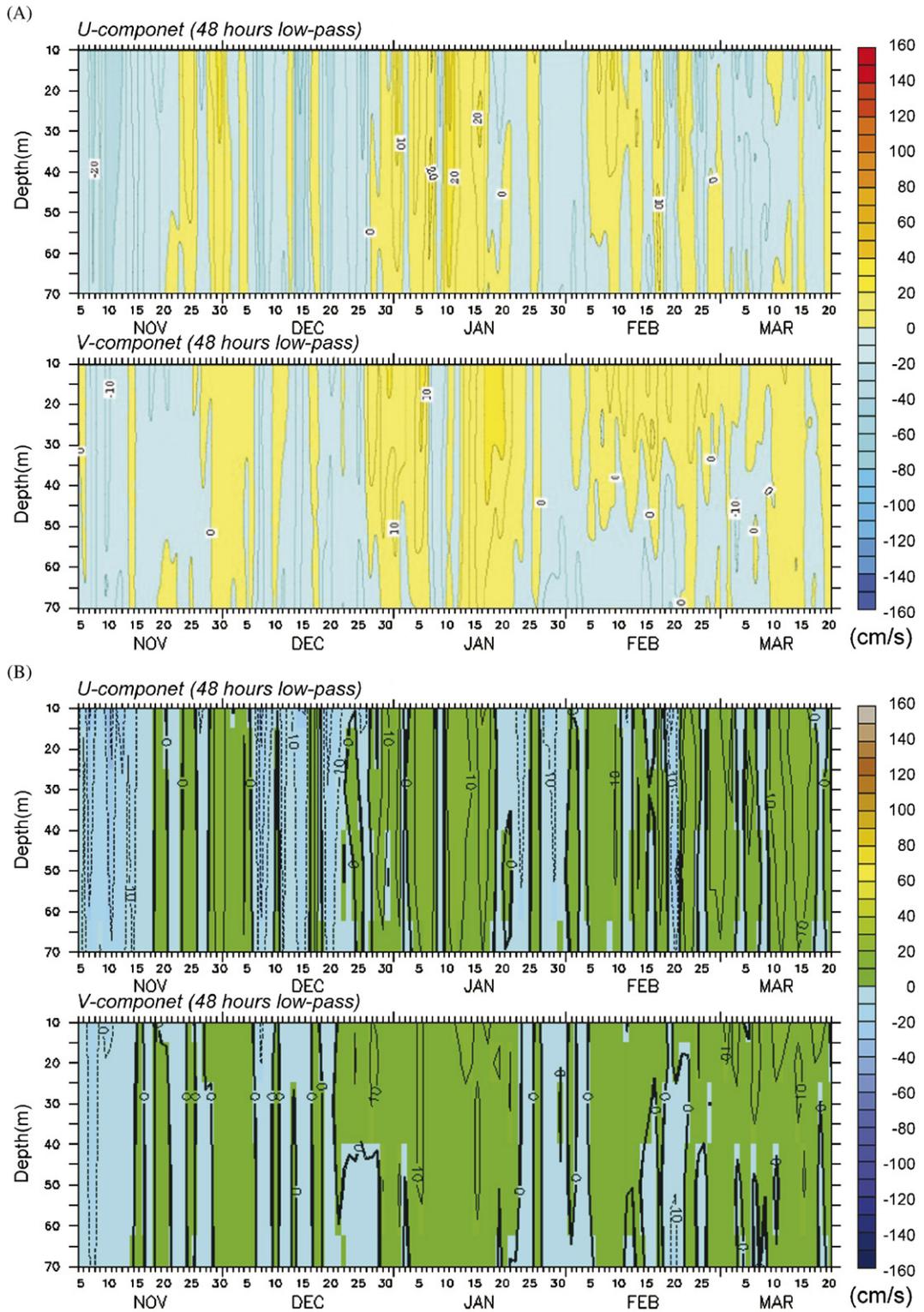
Fig. 2. (A) Observed time series of the 48-h low-pass filtered eastward (*U*) and northward (*V*) velocity components at the T1 station (after Yang, 2006). (B) Model-derived time series of velocity components at the same location of the T1 station. The contour interval is $10 \, \mathrm{cm \, s^{-1}}$.

velocity reproduced a similar pattern of intra-seasonal fluctuations with the observations, except in March 2002 when the model velocity is generally towards the east instead of a westward flow shown in the mooring data. The correlations between mooring and modeled velocity for both U and V during the entire period reach 0.7 with no time lag (Yang, 2006).

In addition to the T1 station, which is on the shelf, we also compare the velocity fields in the deep water. Fig. 3A is the depth-averaged (30–170 m) velocity sticks at the SCS2 station from April 11 to December 4, 1999 (from Liang, 2002). The SCS2 station is in the central SCS at 15.30°N and 115.21°E (see Fig. 1) and its local water depth is around 4250 m. Fig. 3B shows corresponding results derived from the model. Both the velocity sticks show prevailing northward flow at SCS2 with occasional reversals in June and during the period from September to middle October; although there are few discrepancies on both ends of the time series. The similarity between the two time series suggests that the model is capable of capturing major observational features. We will use the model results to further discuss the mesoscale eddy behavior as well as intra-seasonal variations in the northern SCS.

Similar model-data comparison also has been made in the temperature fields. Fig. 4A shows the observed temperature time series at the SEATS station in 2001. The local water depth at SEATS is around 3800 m. The temperature at the surface layer shows annual variation associated with seasonal heating and cooling. The observed temperatures in summer and early fall show surface warming along with the development of a shallow surface mixed layer (shallower than 30 m). The mixed layer depth (MLD) becomes deeper in winter when the prevailing northeasterly monsoon is stronger. For comparison, the model-derived time series of temperature at the same location in 2001 is presented in Fig. 4C. The model results reproduce many of the observed trends in temperature. These include annual variation of temperature at the surface layer, the cooling of surface temperature during winter, and warming water masses during the summer and early fall. Seasonal tendency of model-predicted MLD is also comparable to that of the observed MLD.

In addition to the seasonal variation, intra-seasonal fluctuations (40–120 days) are dominant at the subsurface thermocline layer. For example, Fig. 4B zooms in an episode from February to March, 2001 when the relatively cold subsurface
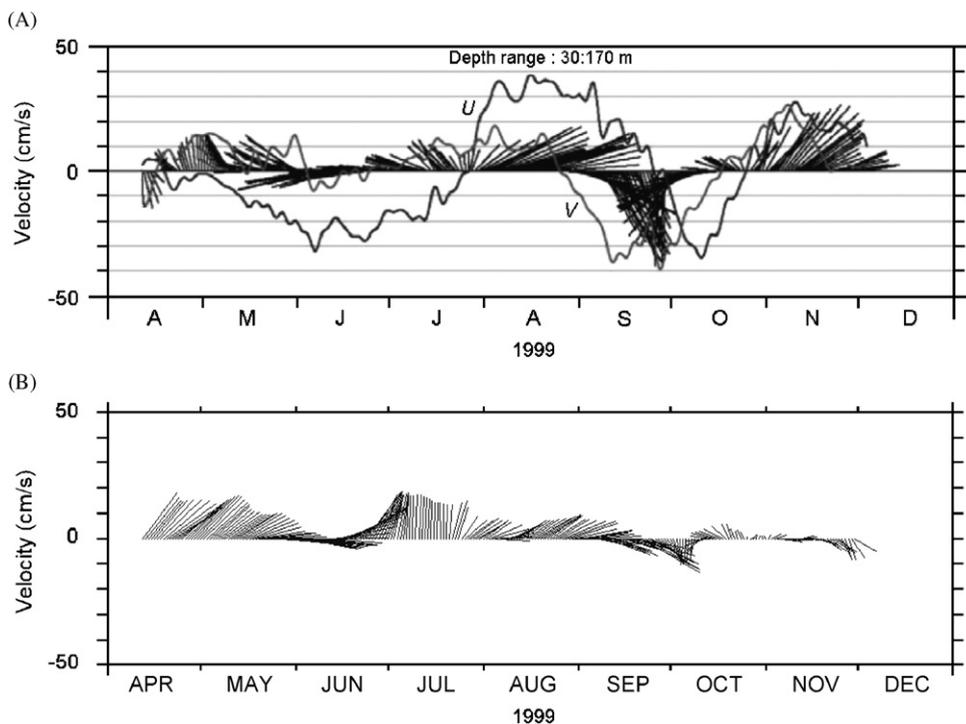
Fig. 3. (A) Stick plot of the depth-averaged current velocity at SCS2, both U and V components are also included (after Liang, 2002). (B) The corresponding results derived from the model.
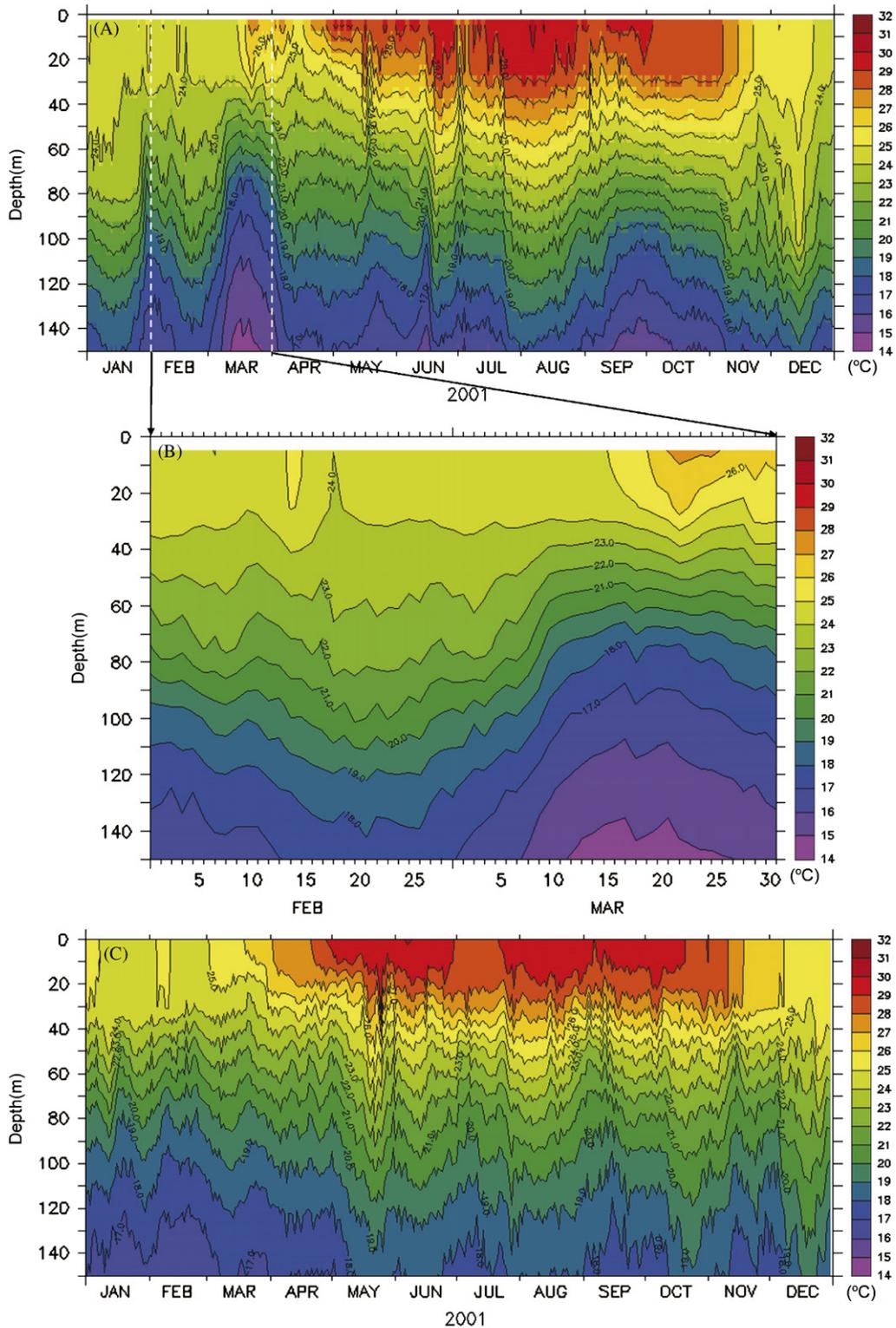
Fig. 4. (A) Observed time series of temperature at the SEATS station in 2001. (B) The 2-month episode from February to March at SEATS. (C) Model-derived time series of temperature at the same location in 2001.

water suddenly becomes much warmer. Significant intra-seasonal fluctuations also are reproduced in the simulated subsurface temperature field. Obviously, this intra-seasonal fluctuation is not caused by the seasonal reversal of the monsoonal winds. What causes the intra-seasonal variation in the area deserves to be further examined. Several possible factors have been attributed to the intra-seasonal variation, including the variability of local wind forcing and the mesoscale eddies. The spectrum of 5-year QSCAT/NCEP wind data over a square between 18°–20°N and 121°–123°E shows no significant intra-seasonal signal in the area (figure not shown), suggesting that the intra-seasonal variation is not driven by the local wind forcing. On the other hand, the model result shows that intra-seasonal variation in the area is caused by mesoscale eddies. The model Kuroshio occasionally makes a loop within the Luzon Strait, forming mesoscale eddies in the intrusion. The scenario that mesoscale eddies propagate westward and cause intra-seasonal variation in the SEATS station is examined in detail in the next section.

3.2. Eddies modulating the hydrography and circulation

Snapshots of sequential model-derived SSHA are shown in Fig. 5 from February 9 to March 24, 2001. The successive eddy motions indicate that the propagation of mesoscale eddies was primarily southwestward. On February 9, the periphery of 'Eddy A' centered at 17.5°N and 115.5°E was visible near the SEATS station, while another cold-core eddy, 'Eddy B', appeared off northwest Luzon (Fig. 5A). The cyclonic cold-core 'Eddy A' affected and decreased the subsurface temperature of the SEATS station (see Fig. 4B). Both 'Eddy A' and 'Eddy B' propagated southwestward and 'Eddy A' gradually moved away from the SEATS station. On February 25, the SEATS station was free from the influence of 'Eddy A' and was surrounded by warmer water (Fig. 5B), resulting in the increased temperature at the SEATS station, as shown in Fig. 4B. The southwestward-propagating 'Eddy A' moved away from the SEATS station; meanwhile, 'Eddy B' came near on March 8 (Fig. 5C). 'Eddy B' reached the SEATS station on March 24 (Fig. 5D), and, again, the subsurface temperature of the SEATS station was decreased (Fig. 4B). Also, the shape and the size of both 'Eddy A' and 'Eddy B' varied during their propagation. Their shapes were

not circular if we regard the zero-contour in Fig. 5 as the edge of the eddy.

A temperature cross-section through the SEATS station and both 'Eddy A' and 'Eddy B' on February 25 is shown in Fig. 6 to demonstrate the eddy structure. The section follows the broken line in Fig. 5B. There are two regions with bulging isotherms. One extended from 114°E to 115°E represents 'Eddy A', and another centered around 118°E is 'Eddy B'. Both eddies can be traced down to 300 m below the surface. As mentioned earlier, the temperature at SEATS gradually becomes warmer when it is away from the influence of the cold-core 'Eddy A'.

The propagation of mesoscale eddies was also evident in the gridded altimeter SSHA from Center for Archiving, Validation and Interpretation of Satellite Data in Oceanography, the French Space Agency [Archiving, Validation, and Interpretation of Satellite Data in Oceanography (AVISO), 1992], which further confirms the model result. The SSHA indicated no eddy at the SEATS station on February 28, 2001, but a cold eddy on March 21, 2001 (Fig. 7). Although the spatial pattern does not look very much alike, the phenomenon is comparable to the model simulation. The southwestward-propagation of mesoscale eddies also was evident in AVISO's images.

Furthermore, the center of 'Eddy A' was located at about 17.5°N and 115.5°E on February 9, and the center moved to 17.5°N and 112°E on March 24 (see Fig. 5). This leads to an averaged propagating speed of about 9.0 km day^{-1} (0.1 m s^{-1}) for 'eddy A'. The center of 'Eddy B' was at about 20°N and 119°E, and moved to 19°N and 116.1°E during the time spanning, with an estimated averaged propagating speed of about 7.9 km day^{-1} (0.09 m s^{-1}). The westward propagation speed of the eddies was around 0.09–0.1 m s^{-1}, which was the same order of the propagation speed of a baroclinic Rossby wave in this area (~0.1 m s^{-1}; e.g., Wu et al., 2005), suggesting that long Rossby waves should have a great consequence on the eddies over the study region. The result is basically consistent with the study of mesoscale eddies over the Subtropical Countercurrent (STCC) (Hwang et al., 2004). Hwang et al. (2004) used TOPEX/POSEIDON (T/P) altimetry data to track mesoscale eddies over the STCC and found that the mesoscale eddies propagated at about the Rossby wave speed. Roemmich and Gilson (2001) identified eddies based not only on T/P altimetry but also high-resolution XBT
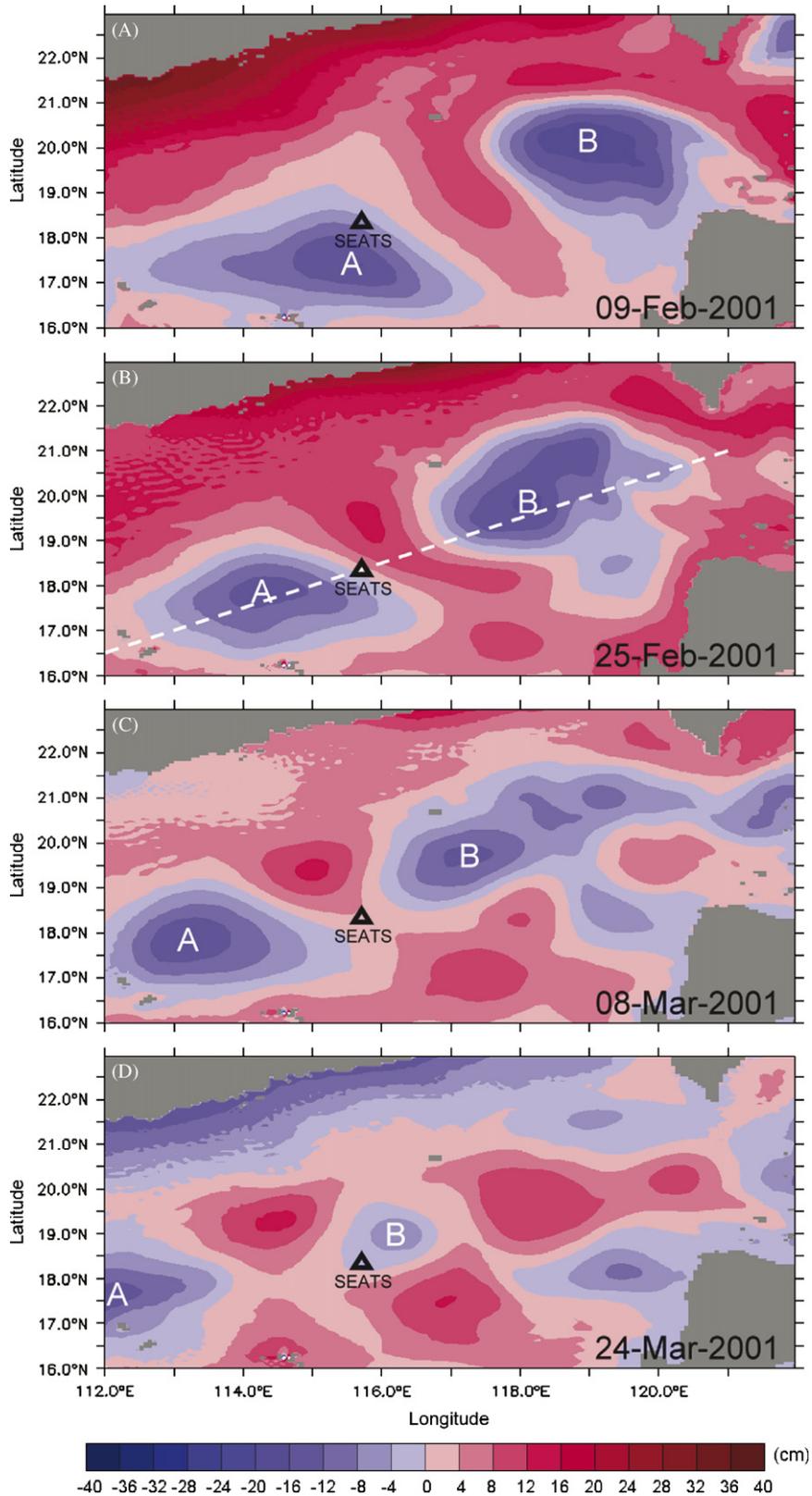
Fig. 5. Snapshots of the sequential model-derived sea-surface height anomaly during the period from February 9, 2001 to March 24, 2001: (A) February 9, (B) February 25, (C) March 8, and (D) March 24. The contour interval is 4 cm.
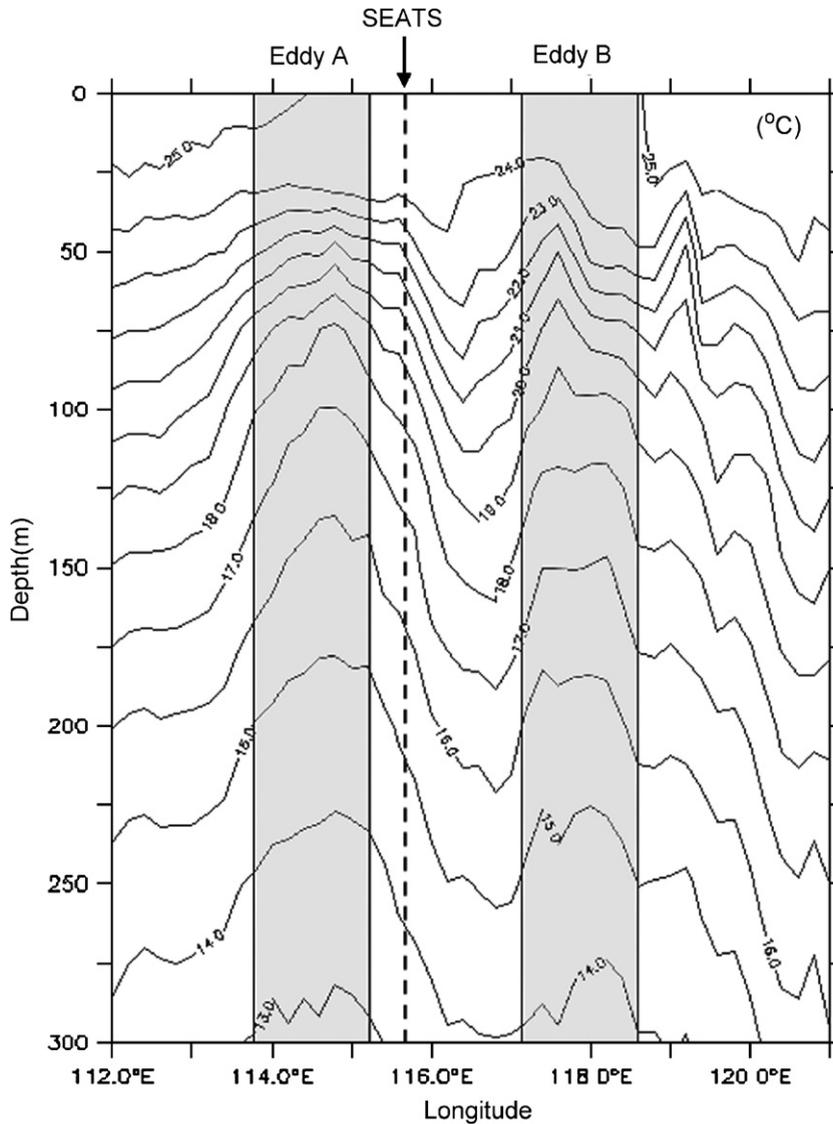
Fig. 6. Cross-section of the model-derived temperature along the broken line as shown in Fig. 5B. The contour interval is 1 °C. Shading indicates eddy region.

transects in the North Pacific Ocean, at an average latitude of 22°N. Their result demonstrated that mesoscale eddies move thousands of kilometers to the west at about 0.1 m s^{-1} at 20°N. This propagating speed is consistent with the present study based on model-derived SSHA.

3.3. Statistics of eddies over the Luzon Strait

We have identified eddies over the Luzon Strait region from January 1, 1999 to December 31, 2003 using model sea-surface heights and velocity fields. Table 1a shows the dates when eddies appeared, and

Table 1b shows the number of eddies in the summer (June, July, and August) and winter (October, November, and December). These eddies are based on visual inspection of the model sea-surface height contours and velocity fields. Table 1a shows that the number of eddies in 2002 is relatively small compared to the other years, while the most eddies exist in 2000. This inter-annual variability might be related to ENSO. In the 5-year period, the Niño 3.4 SST index (5°S–5°N; 170°W–120°W) peaked in November 2002 in response to an El Niño event in the tropic Pacific. On the other hand, the winter of 2000 was a La Niña episode based on the
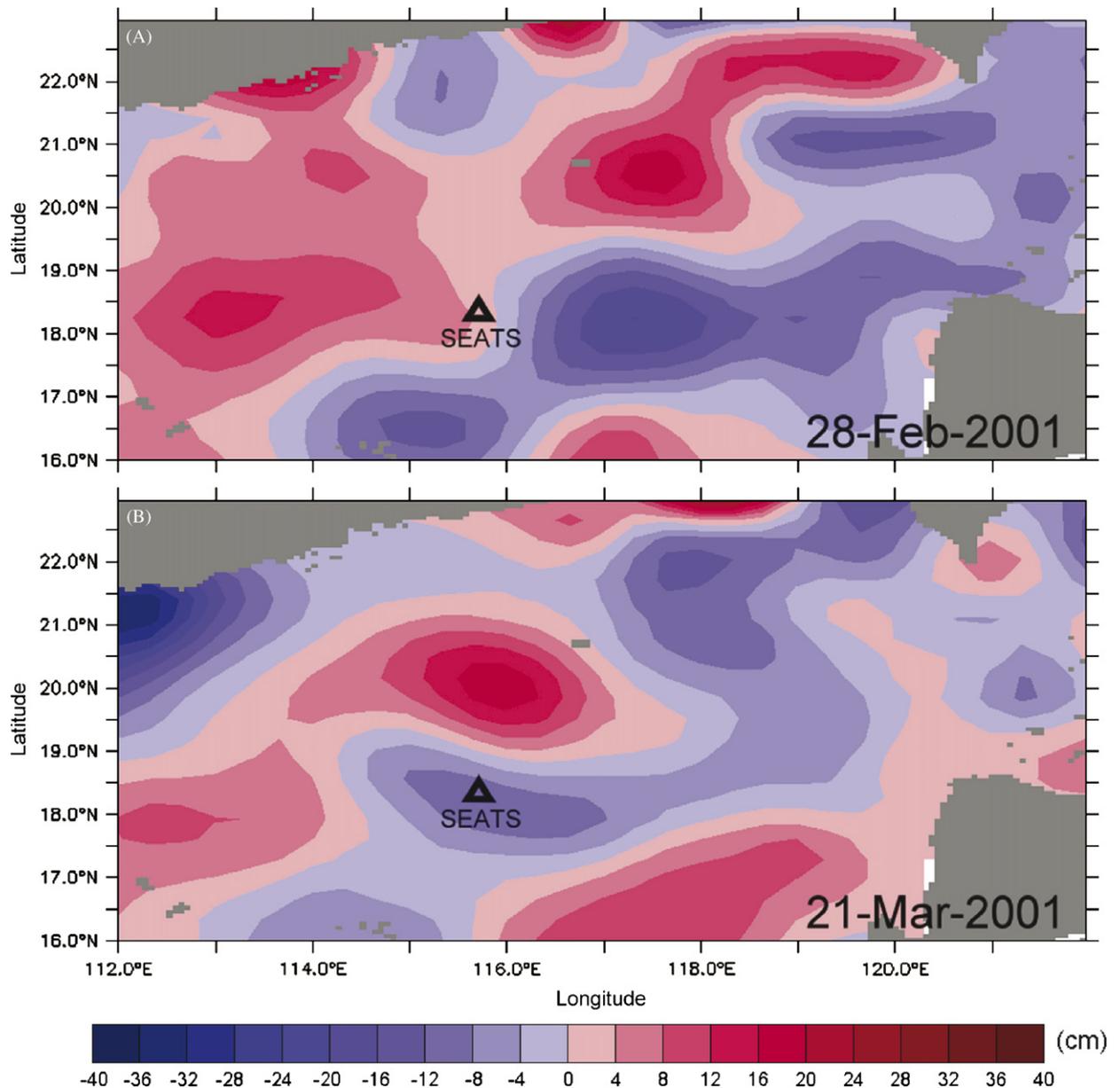
Fig. 7. The AVISO's satellite images on (A) February 28 and (B) March 21, 2001. The contour interval is 4 cm.

criterion that the SST anomaly is less than $-0.5\,^\circ$C in the Niño 3.4 SST index.

In addition to year-to-year variations, Table 1a also shows that the time intervals between two sequential eddies contain a seasonal variation. In general, the time interval is smaller during winter than in other seasons. The time interval is around 30–55 days during winter time while it is around 75–110 days during summer time. Therefore, the number of eddies in winter is much larger than in

summer as shown in Table 1b. There are always two eddies existing during winter time (October, November, and December), but only one or even no eddy is present during summer time (June, July, and August). The AVISO satellite images confirm this finding. Table 2 presents the eddy numbers in summer and winter based on the AVISO SSHA. Again, the eddy number in summer is significantly reduced than that in winter. This seasonal variability is obviously correlated with the variation of

Table 1
(a) The appeared dates of eddies from model simulation and (b) the number of eddies in the summer (June, July, and August) and winter (October, November, and December)

Year	The appeared dates of eddies						
(a)							
1999	02/27	03/23	05/19	08/23	10/10	12/06	
2000	02/06	03/19	05/18	08/04	09/27	11/23	12/20
2001	01/19	03/29	05/25	09/13	11/12	12/27	
2002	02/15	03/11	09/01	11/06			
2003	02/06	04/25	10/07	11/15	12/24		
	Number of eddies						
	Summer (JJA)	Winter (OND)					
(b)							
1999	1	2					
2000	1	2					
2001	0	2					
2002	0	1					
2003	0	3					
Total	2	10					

Table 2
Same as Table 1b but eddies are based on visual inspections of the AVISO's SSHA

Year	Numbers of eddies	
	Summer (JJA)	Winter (OND)
1999	0	1
2000	1	2
2001	1	2
2002	0	2
2003	0	2
Total	2	9

Kuroshio intrusion. Eddies are more often in winter than in summer, which means that more Kuroshio intrusion takes place during winter. The 5-year average of the model velocity at 50-m in December and August shown in Fig. 8A and B demonstrates this different intrusion process.

Model result reproduces several observational features in December (Fig. 8A). For example, the model result shows a low-velocity region off the southeast tip of Taiwan, which is consistent with the fact that the Argos satellite-tracked drifters were trapped in this region before rejoining the north-ward-flowing Kuroshio (Centurioni et al., 2004). Also, the model indicates that the largest westward component of the Kuroshio intrusion is through the deepest channels of the Luzon Strait (the Balintany

Channel, and south of Babuyan Island) and the largest eastward component (outflow back toward the Philippine Sea) is through the Bashi Channel between southern Taiwan and Batan Island. These features are in agreement with the previous findings from both drifter data (Centurioni et al., 2004, Fig. 5) and composite ship-board ADCP data (Liang et al., 2003, Fig. 12).

Model result for August shows a similar Kur-oshio intrusion path to that in December (Fig. 8B). However, the westward component of the intrusion through the Balintany Channel in August was much smaller than in December. This seasonal variability is consistent with the previous findings that the Kuroshio intrusion into the interior of the SCS is mainly between October and January (e.g., Shaw, 1991; Qu, 2002; Centurioni et al., 2004). For example, based on an analysis of a hydrographic data set, Shaw (1991) demonstrated that the Philippine Sea Water stretched west as far as 115°E and along the continental margin south of China from October to January. Qu (2002) reached similar conclusions about intrusions upon inspec-tion of the distribution of oxygen concentration. Centurioni et al. (2004) also found that drifters crossed the Luzon Strait and reached the interior of the SCS only between October and January, with ensemble mean speeds of $0.7 \pm 0.4 \, \mathrm{m \, s^{-1}}$.

It is well known that eddies could develop as a result of barotropic instabilities associated with
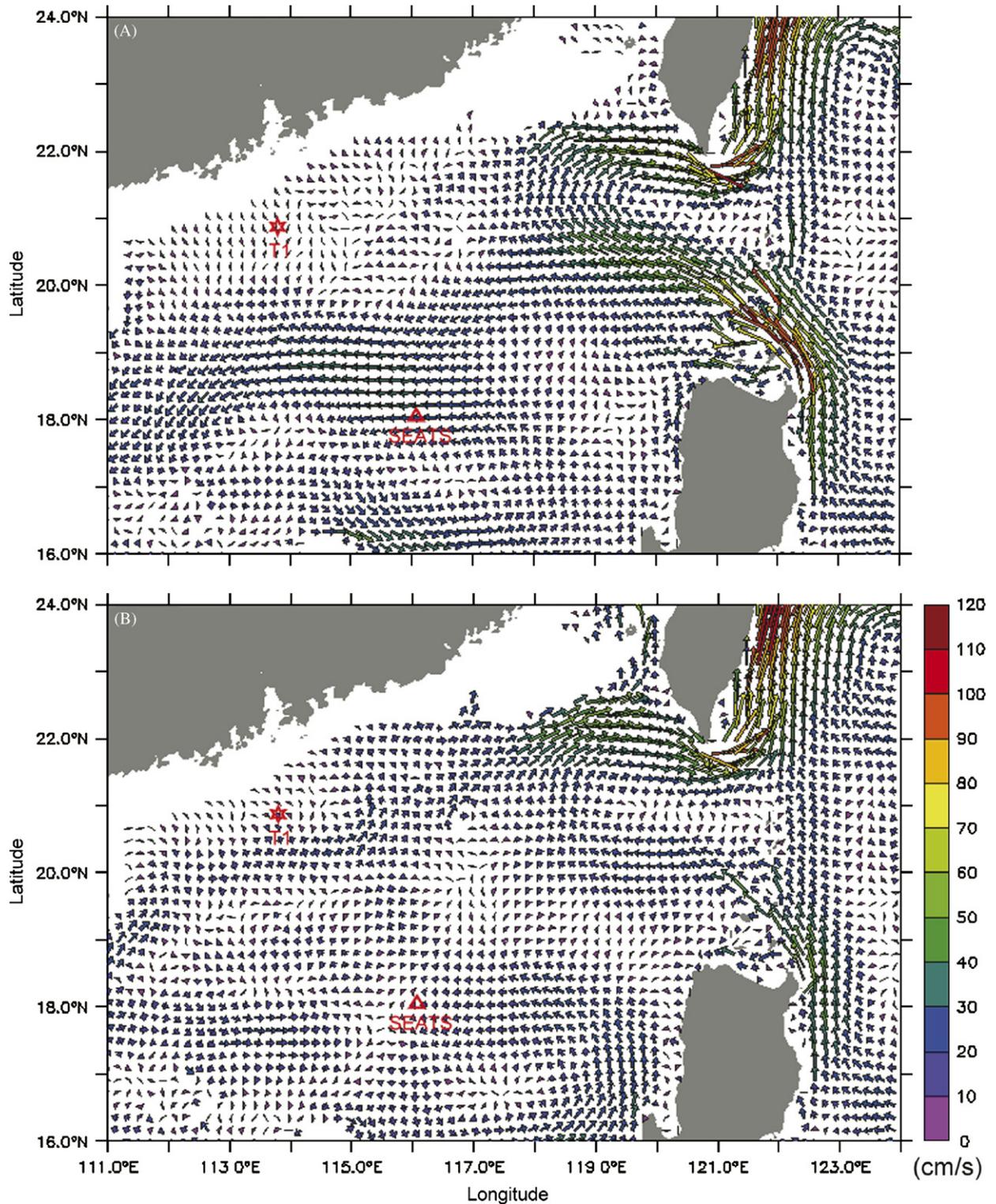
Fig. 8. The five-year average of the model-derived velocity at 50 m depth in (A) December and (B) August, respectively.
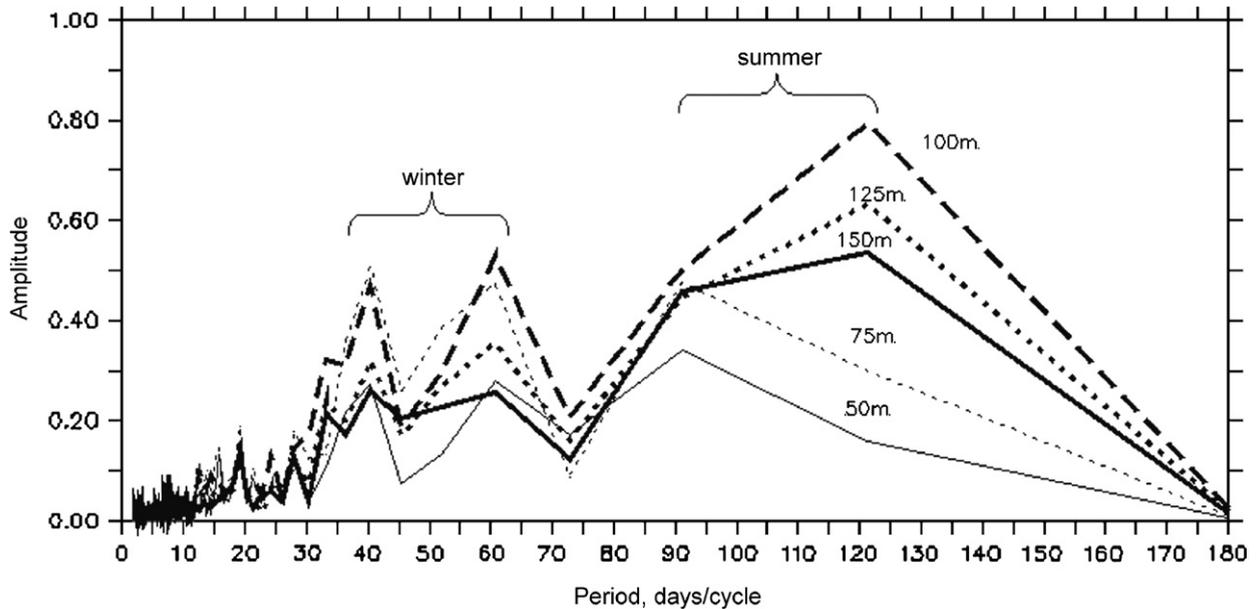
Fig. 9. The temperature amplitude spectrum of the SEATS station.

lateral current shears. Lateral variations in velocity of Kuroshio within the Balintany Channel caused by friction with coastal boundary are capable of periodically forming eddies. These eddies pinch from the Kuroshio and generate prominent temporal and spatial variability in regional hydrography and circulation. The frequency (or period) of eddy shedding can be quantified from the so-called Strouhal number derived from laboratory experiments. The period of eddy shedding can be calculated as follows by applying the related data:

$$S_t = \frac{w}{T\overline{U}} = 0.163 \pm 0.01 \qquad (2)$$

for a cylinder (Sarpkaya and Isaacson, 1981), where S_t is the Strouhal number, T the period of eddy shedding, w the width of the Luzon Strait ($\sim$350 km), and $\overline{U}$ the mean velocity of the upstream of the intrusion current, which is averaged over a $1° \times 1°$ box from 122°E to 123°E and from 17.5°N to 18.5°N. The 5-year average velocity in December is about 50–60 cm s^{-1} (see Fig. 8A); hence, the corresponding period is around 40–50 days. On the other hand, the five-year average velocity in August is about 20–30 cm s^{-1} (Fig. 8B), and the corresponding period is around 80–120 days. These estimates are consistent with the model results. Furthermore, these periods are most prominent at the subsurface thermocline layer as shown in temperature amplitude spectrum of the SEATS

station (Fig. 9). This supports the hypothesis that intra-seasonal temperature fluctuations found in the SEATS station are due to modulation by mesoscale eddies generated around the Luzon Strait.

4. Conclusions

The present model was compared with observed time series of temperature from the SEATS station and velocity from two bottom-mounted ADCPs in the SCS. The intra-seasonal fluctuations shown in both the observed and simulated temperature fields are attributed to the mesoscale eddies that originate in the vicinity of the Luzon Strait. The model result shows that the Kuroshio occasionally makes a loop within the Luzon Strait forming mesoscale eddies in the intrusion. These mesoscale eddies propagate westward and modulate the hydrography and circulation in the area. The mesoscale eddies have the same propagation speed as baroclinic Rossby waves ($\sim$0.1 m s^{-1}).

The simulated velocity fields also reproduce the intrusion path of the Kuroshio and its seasonal variability. The seasonal variability is consistent with the previous findings that the Kuroshio intrusion into the interior of the SCS mainly takes place during winter time, so that the number of eddies in winter is much larger than in the summer. The periods of eddy shedding estimated from the Strouhal number are around 40–50 days in December, and about

80–120 days in August, respectively. These periods are discernible at the subsurface thermocline layer of the SEATS station, further confirming that the intra-seasonal fluctuations presented in the SEATS station are the manifestation of westward-propagating mesoscale eddies generated in the vicinity of the Luzon Strait.

Acknowledgments

References

Archiving, Validation, and Interpretation of Satellite Data in Oceanography (AVISO), 1992. AVISO User Handbook: Merged TOPEX/Poseidon Products, Rep. AVI-NT-02-202-CN, ed. 2.1, Cent. D'Etudes Spatiales, Toulous, France.

Blumberg, A.F., Mellor, G.L., 1987. A description of a three-dimensional coastal ocean circulation model. In: Heaps, N.S. (Ed.), Coastal and Estuarine Sciences 4: Three Dimensional Coastal Models. AGU, Washington, DC, pp. 1–16.

Centurioni, L.R., Niiler, P.P., Lee, D.-K., 2004. Observations of inflow of Philippine Sea Water into the South China Sea through the Luzon Strait. Journal of Physical Oceanography 34, 113–121.

Farris, A., Wimbush, M., 1996. Wind-induced intrusion into the South China Sea. Journal of Oceanography 52, 771–784.

Flather, R.A., 1976. A tidal model of the north–west European continental shelf. Memories de la Society Royal des Sciences de Liege 6 (10), 141–164.

Hwang, C., Wu, C.-R., Kao, R., 2004. TOPEX/Poseidon observations of mesoscale eddies over the Subtropical Counter Current: kinematic characteristics of an anticyclonic eddy and a cyclonic eddy. Journal of Geophysical Research 109, C08013, doi:10.1029/2003JC002026.

Li, L., Nowlin, W.D., Jilan, S., 1998. Anticyclonic rings from the Kuroshio in the South China Sea. Deep-Sea Research 45A, 1469–1482.

Liang, W.-D., 2002. Study of upper ocean thermal and current variation in the South China Sea. Ph.D. Dissertation, National Taiwan University, 125pp.

Liang, W.-D., Tang, T.Y., Yang, Y.J., Ko, M.T., Chuang, W.-S., 2003. Upper-ocean currents around Taiwan. Deep-Sea Research II 50, 1085–1105.

Mellor, G.L., Yamada, T., 1982. Development of a turbulence closure model for geophysical fluid problems. Review of Geophysics and Space Physics 20, 851–875.

Metzger, E.J., Hurlburt, H.E., 2001. The nondeterministic nature of Kuroshio penetration and eddy shedding in the South China Sea. Journal of Physical Oceanography 31, 1712–1732.

Milliff, R.F., Large, W.G., Morzel, J., Danabasoglu, G., Chin, T.M., 1999. Ocean general circulation model sensitivity to forcing from scatterometer winds. Journal of Geophysical Research 104, 11337–11358.

Nitani, H., 1972. Beginning of the Kuroshio. In: Stommel, H., Yoshida, K. (Eds.), Kuroshio, Physical Aspects of the Japan Current. University of Washington Press, Washington, DC, pp. 129–163.

Qu, T., 2000. Upper-layer circulation in the South China Sea. Journal of Physical Oceanography 30, 1450–1460.

Qu, T., 2002. Evidence for water exchange between the South China Sea and the Pacific Ocean through the Luzon Strait. Acta Oceanologica Sinica 21, 175–185.

Qu, T., Lukas, R., 2003. The bifurcation of the North Equatorial Current in the Pacific. Journal of Physical Oceanography 33, 5–18.

Roemmich, D., Gilson, J., 2001. Eddy transport of heat and thermocline waters in the North Pacific: a key to interannual/decadal climate variability. Journal of Physical Oceanography 31, 675–687.

Sarpkaya, T., Isaacson, M., 1981. Mechanics of wave forced on offshore structures. Van Nostrand Reinhold Company, New York.

Shaw, P., 1991. The seasonal variation of the intrusion of the Philippine Sea water into the South China Sea. Journal of Geophysical Research 96, 821–827.

Smagorinsky, J., 1963. General circulation experiments with the primitive equations. I. The basic experiments. Monthly Weather Review 91, 99–164.

Wu, C.-R., Chang, C.-W.J., 2005. Interannual variability of the South China Sea in a data assimilation model. Geophysical Research Letters 32 L17611, doi:10.1029/2005GL023798.

Wu, C.-R., Hsin, Y.-C., 2005. Volume transport through the Taiwan Strait: a numerical study. Terrestrial, Atmospheric and Oceanic Sciences 16 (2), 377–391.

Wu, C.-R., Tang, T.Y., Lin, S.F., 2005. Intra-seasonal variation in the velocity field of the northeastern South China Sea. Continental Shelf Research 25, 2075–2083.

Yang, K.-C., 2006. The non-persistent South China Sea warm current. Master dissertation, National Taiwan University, 48pp.